Journal of Chromatography A, 1218 (2011) 4160–4166

Contents lists available at ScienceDirect

Journal of Chromatography A

journal homepage: www.elsevier.com/locate/chroma

Processing nanoparticles with A4F-SAXS for toxicological studies: Iron oxide in cell-based assays

Patrick Knappe[a], Linda Boehmert[b], Ralf Bienert[a], Silvana Karmutzki[b], Birgit Niemann[b], Alfonso Lampen[b], Andreas F. Thünemann[a,*]

[a] BAM Federal Institute for Materials Research and Testing, Richard-Willstätter-Str. 11, 12489 Berlin, Germany
[b] BfR Federal Institute for Risk Assessment, Thielallee 88-92, 14195 Berlin, Germany

ARTICLE INFO

Article history:
Available online 16 November 2010

Keywords:
Field-flow-fractionation
Small-angle X-ray scattering
Nanoparticle

ABSTRACT

Nanoparticles are not typically ready-to-use for *in vitro* cell culture assays. Prior to their use in assays, powder samples containing nanoparticles must be dispersed, de-agglomerated, fractionated by size, and characterized with respect to size and size distribution. For this purpose we report exemplarily on polyphosphate-stabilized iron oxide nanoparticles in aqueous suspension. Fractionation and online particle size analysis was performed in a time-saving procedure lasting 50 min by combining asymmetrical flow field-flow fractionation (A4F) and small-angle X-ray scattering (SAXS). Narrowly distributed nanoparticle fractions with radii of gyration (R_g) from 7 to 21 nm were obtained from polydisperse samples. The A4F-SAXS combination is introduced for the preparation of well-characterized sample fractions originating from a highly polydisperse system as typically found in engineered nanoparticles. A4F-SAXS processed particles are ready-to-use for toxicological studies. The results of preliminary tests of the effects of fractionated iron oxide nanoparticles with a R_g of 15 nm on a human colon model cell line are reported.

1. Introduction

Nanoparticles have been used routinely as ingredients in modern materials, food packaging, agriculture, and medical applications for years [1]. In the European Union, iron oxide compounds are authorized as the food colorant E172 and used, for example, to color drageés, olives, cheese rinds and as component in pharmaceutical and cosmetic formulations. Food colorants are tested for safety and therefore iron oxides can be used in the arbitrary amounts required to achieve the desired color. If nanoparticles are used, a safety reevaluation of the food colorants is requested by the Federal Institute for Risk Assessment of Germany, because nanoparticles frequently exhibit quite different characteristics than their bulk forms as a consequence of their small size and large surface to volume ratio. They, therefore, have the potential to change their bioavailability and toxicity [2–4].

Up to now, no mandatory regulations regimenting the countless applications for nanoparticles in the scope of industry [5] exist although, along with their benefits [3], serious concerns have arisen about safety risks to human health and the environment [6–10]. Despite these considerations, nanoparticle toxicity specifications are typically based on the effects of the corresponding bulk material properties. Many current studies on nanoparticle toxicity deal with samples that have not been well physico-chemically characterized and in which the particles exhibit a broad size distribution. This situation is problematic since it is known that particle properties can vary remarkably if the sizes are reduced even within the 100–1 nm range [11–14]. Thus, extensive studies of the biological properties of nanoparticles and materials containing nanoparticles are needed. Such studies should focus on size, size distribution (granulometry), and shape, in addition to chemical composition and surface chemistry because these issues are considered to be fundamental parameters of their effectiveness [15]. Unfortunately, many commercial nanoparticles are received as powders which cannot be totally broken up into primary particles by ultrasound or chemical dispersants [16]. In addition, the nanoparticles typically exhibit broad size distributions as a result of their production process. Therefore, to yield reliable and unambiguous results when testing the effects of nanoparticles on living cells, particle samples of narrow size distribution are needed to account for size-specific properties.

The aim of this study is the size separation and characterization of a given polydisperse sample of dispersed nanoparticles. We will show that this can be achieved by means of online coupling of asymmetric flow field-flow fractionation (A4F) with small-angle X-ray scattering (SAXS) [17,18]. The setup is shown in Fig. 1. In

* Corresponding author. Tel.: +49 3081041130.
E-mail addresses: patrick.knappe@bam.de (P. Knappe), linda.boehmert@bfr.bund.de (L. Boehmert), andreas.thuenemann@bam.de (A.F. Thünemann).

0021-9673/$ – see front matter © 2010 Elsevier B.V. All rights reserved.
doi:10.1016/j.chroma.2010.11.012

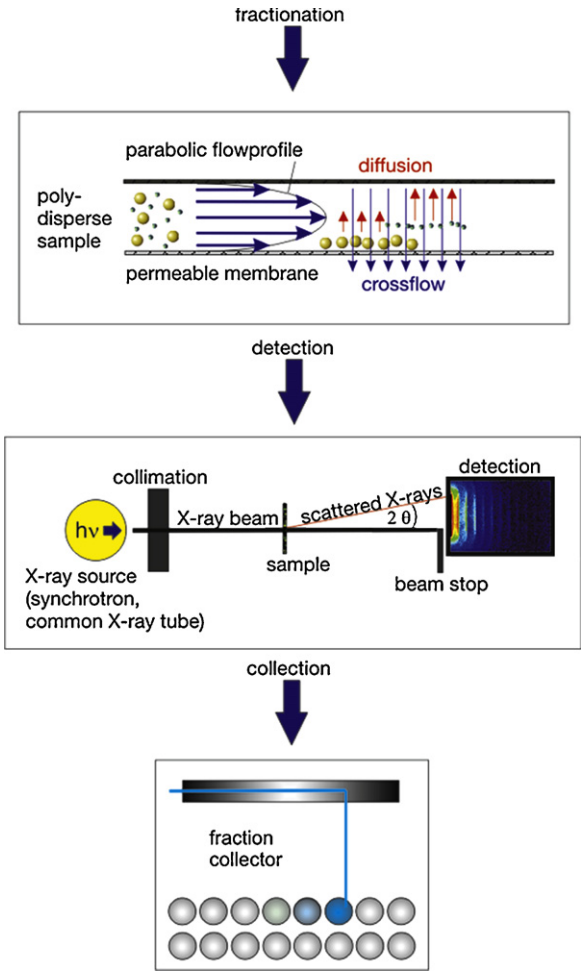

Fig. 1. A4F-SAXS setup consisting of A4F, SAXS instrument, and sample collector (from top to bottom). First, the samples are separated sequentially from smallest to largest particles in the A4F (top). The A4F outlet is connected directly to a flow capillary of the SAXS instrument where the scattered X-rays are monitored with a CCD detector for a time period that corresponds to the desired volume of one sample fraction (middle). The sampling frequency of the present study was one fraction per 60 s. Finally, the SAXS flow capillary is connected to a sample fraction collector (bottom).

this context the A4F functions as a gentle separation technique, based on different diffusion coefficients of the analyte components only [19]. The theoretical background is described in detail elsewhere [19–21]. A4F is suitable for the separation of particles over an exceptionally wide size range of 1 nm up to the micrometer scale. By varying the crossflow decay profile, this method can be adapted individually to optimize separation conditions for each sample. Dilution of the samples during fractionation can be reduced significantly by implementing a slot outlet function [22]. As a result, samples are yielded with concentrations directly applicable for testing of their biological activities.

With small-angle X-ray scattering the whole particle ensemble in the probed sample volume is measured, and therefore, the data for particles sizes are inherently statistically significant. Although SAXS is very accurate for narrowly size-distributed particle samples in the range of 1–100 nm, high polydispersity of the sample will often yield ambiguous results [17,18,23,24]. For this reason the size-fractionation of sodium polyphosphate ("Grahams salt") stabilized iron oxide nanoparticle suspensions provided by A4F is also necessary in our work before recording SAXS curves.

The gastrointestinal tract is the first barrier after oral uptake of nanoparticles. However, there is very little information available regarding cellular effects of iron oxide nanoparticles on cells representing intestinal functions. We choose this non-toxic polyphoshate-stabilizing agent for reasons of biocompatibility [25]. The human Caco-2 cells represents a well accepted model for human intestinal cells reflecting many functions of the intestine [26]. Therefore, the impact of the nanoparticles on cellular effects on human Caco-2 cells was investigated. Cell viability was tested by Cell Titer-Blue® assays and DAPI staining after incubation of these cells with different concentrations of nanoparticles in the culture medium.

2. Materials and methods

2.1. Materials

Fe_2O_3-nanopowder (maghemite, 99.5%) with nominal radii of 10–20 nm (specified from TEM pictures by the manufacturer) was obtained from IoLiTec (D-74076 Heilbronn). Sodium polyphosphate ($(NaPO_3)_x$, "Grahams salt") was obtained from Riedel de Haën. Deionized water for solvent preparation obtained from a Millipore®-system was used. The solvent solution was filtered again through a 0.1 μm cellulose filter prior to use to avoid dust in the sample.

In all 800 mg of the Fe_2O_3 nanoparticles were suspended in 10 mL of a 0.1% (w/v) aqueous solution of sodium polyphosphate and sonicated (60 s, 50% cycle, 56 W) using a SONOPULS HD 2070 from the Bandelin GmbH. The resulting suspension was centrifuged (60 s, 80 × *g*) in a Heraeus centrifuge, and the supernatant was filtrated successively through 450 nm and 200 nm sterile syringe PES-filters.

2.2. Methods

The A4F unit was purchased from Postnova Analytics GmbH (Germany), and consists of an AF2000 focus system, equipped with PN 5200 auto sampler, PN 7505 inline degaser, PN 1122 tip, and focus pump. Inline solvent filters were placed between the pumps and the channel to reduce background noise. The channel thickness was 500 μm, and the membrane consists of regenerated cellulose (RC) with a molecular weight cut-off (MWCO) of 10^4 g mol^{-1}. The solvent used was water, containing 0.1% (w/v) sodium polyphosphate as electrolyte. The flow rates were controlled via AF2000 software (Postnova). A slot-outlet function was implemented by using a modified channel top with an additional port 13 mm in front of the laminar outlet port [22] and by connecting a narrow capillary to the slot outlet port of the A4F unit to achieve 80% slot flow as a result of backpressure. An UV detector (Milton Roy, detection at wavelength of 400 nm) was coupled directly to the channel outlet. The fractionation and measurements were performed at 20 ± 1 °C. After SAXS detection, a fraction collector (Gilson) was additionally connected. A sample of 200 μL with an iron oxide content of 5.6 ± 0.3 mg mL^{-1} was injected. The fractionation procedure was repeated several times to yield a sufficient volume of sample material.

For SAXS measurements a Kratky-type instrument was used. It has a small sample-to-detector distance of 309 mm and is therefore suitable for investigation of dispersions with even low scattering intensities (SAXSess from Anton Paar, Austria). For online detection a flow capillary was connected directly to the UV detector outlet. The measured intensity was corrected by subtracting the scattering intensity of the capillary filled with pure solvent. A common X-ray tube was used as X-ray source, emitting Cu K_α radiation ($\lambda = 0.154$ nm). The scattering vector q is defined in terms of the scattering angle θ and the wavelength, thus $q = 4\pi/\lambda \sin\theta$. Deconvolution (slit length desmearing) of the SAXS curves

was performed using SAXSQuant software provided by Anton Paar.

The quantification of the iron oxide concentration in the samples was performed by dissolution of an aliquot of the fractions in HCl; this was fluorometrically quantified using the Nanocolor® Iron Kit from Macherey–Nagel to measure the iron concentration in the suspensions.

The human colon adenocarcinoma cell line Caco-2 was obtained from the European Collection of Cell Cultures (ECACC, Porton Down, UK). Cells were maintained in Dulbecco's modified Eagle's medium (DMEM, PAN Biotech, Aidenbach, Germany) at 37 °C in a humidified atmosphere of 5% CO_2. All Media were supplemented with 10% (v/v) FCS (fetal calf serum) or 1% (v/v) ITS (insulin, transferrin, selenium) and 1% (v/v) penicillin/streptomycin. Caco-2 cells were cultured in tissue culture flasks for propagation (75 cm^2) and in 96-well plates for experiments.

After exposure of the cells to nanoparticles, cell viability and proliferation of Caco-2 cells was assessed using the Promegas Cell Titer-Blue® (CTB®) Assay and DAPI staining [27]. The CTB cell assay provides a fluorescent method for monitoring cell viability. It is based on the ability of living cells to convert resazurin into resorufin. Nonviable cells rapidly lose metabolic capacity and thus do not generate a fluorescent signal. DAPI is a DNA fluorescent stain, and the amount of DNA is related to the number of cells.

The Caco-2 cells were plated into 96-well plates at a density of 5×10^3 cells per well in 100 μL culture medium and allowed to attach for 24 h before treatment. Subsequently, culture medium was replaced by 100 μL nanoparticle suspensions with concentrations of 5, 10, 25, 50 and 100 μg mL^{-1}. Corresponding sodium polyphosphate controls as well medium controls were performed, and the cells were exposed for 24, 48 and 72 h. Finally, 20 μL CTB was added to each well, incubated for additional 2 h and measured on a micro plate reader with 540 nm excitation and 590 nm emission. After the CTB® cell viability assay the cells were fixed and lysed with methanol. The DNA was stained with 100 μL of 20 μM DAPI for at least 30 min. The resulting fluorescence was measured using a micro plate reader with 380 nm excitation and 460 nm emission. The results were related to the corresponding sodium polyphosphate control, and the medium control was set to 100%. Means and standard deviations were calculated from at least three independent experiments.

3. Results and discussion

3.1. Particle fractionation

Nanoparticles from commercially available iron oxide powder were first suspended and de-agglomerated with an ultrasound device in an aqueous polyphosphate solution. This procedure is not size-selective and produces suspensions of particles with unpredictable, broad size distributions, usually unsuitable for cell culture assays where the particles' size is a parameter that effects the toxicological impact. Therefore, we subsequently performed particle size separation and particle size analysis by means of online coupling of A4F and SAXS after preparing the suspension. Total times of only 3000 s were needed for an A4F-SAXS experiment. In the beginning, after 600 s of sample injection in the A4F and sample focusing, a linear decay of the crossflow rate from 1.5 mL min^{-1} to zero was applied within 900 s; no crossflow was applied thereafter. The fast decrease of applied crossflow was chosen as a compromise between high separation quality and reasonable high concentration of the sample at the channel outlet, where the latter is crucial for the particles' usability in the subsequent cell experiments The channel flow rate was kept constant with 1 mL min^{-1}, whereas the slotflow was set to 0.8 mL min^{-1} to prevent further dilution, resulting in a detector flow rate of 0.2 mL min^{-1}. The crossflow profile is given together with the UV signal in Fig. 2. Most of the nanoparticles were eluted at fractionation times between 1200 and 2400 s as derived from the UV signal and from visible inspection of the collected fractions shown in Fig. 3.

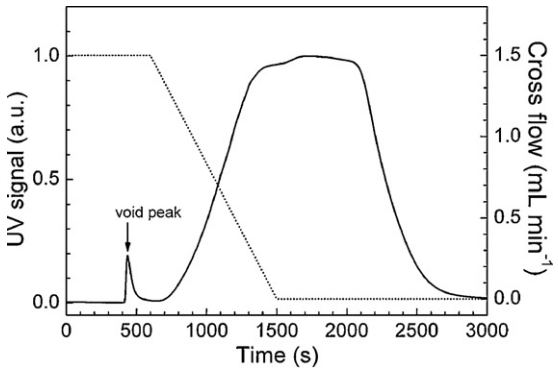

Fig. 2. Elugram of the asymmetric flow field-flow fractionation of polyphosphate stabilized Fe_2O_3 with UV detection at 400 nm. The maximum of the signal is normalized to one (solid line). The crossflow rate decays linearly from 1.5 to 0 mL min^{-1} during elution (dotted line).

3.2. Size analysis of fractionated particles

SAXS curves were recorded online for the fractionation. All fractions display a typical single particle scattering, i.e. no indications of attractive or repulsive interactions were observed. It should be mentioned that the scattering of X-rays in particle dispersions is based on the electron density difference between the dispersant and the particle, in our case water and iron oxide. A shell of the iron oxide particles formed by the polymeric stabilizing agent poly(phosphate) has an electron density similar to the solvent and is therefore not "seen" by SAXS. The particles' core dimension is thus obtained directly.

Fig. 3. Collected fractions of polyphosphate stabilized iron oxide nanoparticles after A4F-SAXS measurement. The fractionation time increases from left to right in sequence with the increasing radii of the particles.

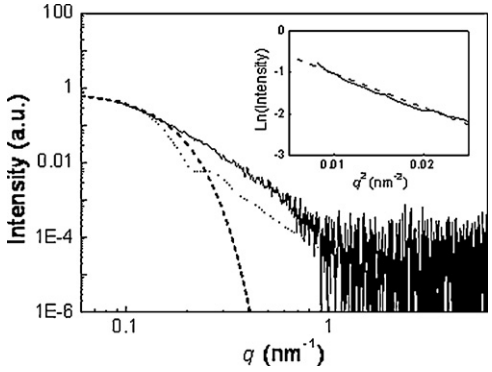

Fig. 4. Scattering curve of fraction number 30 in double logarithmic presentation (solid line), scattering according to Guinier's law in exponential form with R_g = 15.4 nm (dashed line), and the scattering of a solid sphere with the same radius of gyration corresponding to R = 19.9 nm (dotted line). A Gaussian size distribution with a width of 3 nm and an incoherent background of 1.5×10^{-5} was used for simulation. Inset: Classical Guinier plot of the same data at low q-values (solid line) and a linear Guinier fit with R_g = 15.4 nm.

The evaluation of the SAXS data was first performed using the Guinier approximation

$$I(q) = I(0) \cdot \exp\left[-\tfrac{1}{3}R_g^2 q^2\right], \quad \text{with} \quad I(0) \sim (\rho_1 - \rho_2)^2 \cdot V^2 \cdot n, \qquad (1)$$

where $I(0)$ is the extrapolated intensity at zero angle, $(\rho_1 - \rho_2)$ is the electron density difference between the particle and the dispersant, V is the particles volume, and n is the particle number, respectively. The Guinier approximation is applicable for $q \cdot R_g \leq 1.3$ to yield the particles' radius of gyration (Guinier radius, R_g) [28], which can be converted to the corresponding radius of a sphere by $R = (5/3)^{1/2} \cdot R_g$. The scattering data and the corresponding Guinier fit of fraction number 30 are depicted in Fig. 4 as a typical example (solid line in large figure and inset). For comparison the curve fit is shown in its exponential form in the double logarithmic plot (dashed line) and in the classical linear presentation, in an $\ln I - q^2$-plot (dashed line in the inset). The smallest particle sizes were found in fraction 13 with $R_g = 7.0 \pm 0.7$ nm and the largest in fraction 40 with $R_g = 20.6 \pm 0.7$ nm. No significant scattering was detected for fractions with numbers smaller that 12 and larger than 40. The predominant fraction of the particles is centered on R_g = 15-16 nm (R = 19–20 nm) for fractions 25–35. This is apparent as a result of a maximum in the scattering intensity at a fractionation time around 1700 s. An overview on the R_g and the corresponding R-values is given in Table 1 and Fig. 5.

For data interpretation we also tested model curves of spheres with low polydispersity. The scattering of spheres with a radius of 19.9 nm and a Gaussian size distribution with a width of 3 nm is given as an example in Fig. 4. It can be seen that the measured curve and the model curve show significant deviations at q-values between 0.2 and 1.0 nm^{-1}. Model curves using other types of size distributions result in similar deviations. Our finding that simple models of spheres are not satisfactory for interpreting the entire scattering curve is a result of the significantly irregular and edgy shape of the particles as is visible in Fig. 6; this is typi-

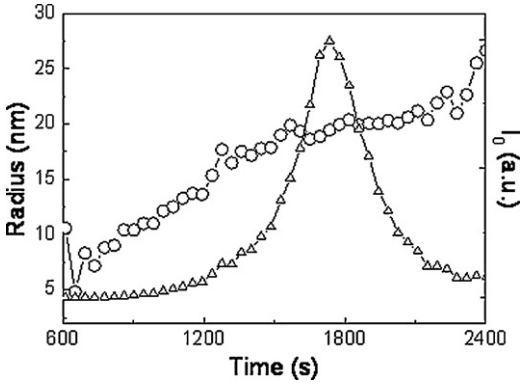

Fig. 5. Results of SAXS analysis using the Guinier approximation according to Eq. (1). Derived radii (circles) and $I(0)$ intensities (triangles) as a function of the fractionation time.

Table 1
Particle size characteristics for fractions of collected nanoparticles after A4F-SAXS online coupling. The radius of gyration R_g was determined according to Eq. (1), and R is the corresponding sphere radius. The particle volume was calculated according to Eq. (2), and R_V is the sphere radius calculated using this value.

Fraction no.	R_g (nm)	R (nm)	Volume (nm^3)	R_V (nm)	Ratio R/R_V
1–12[a]	–	–	–	–	–
13	7.0 ± 0.7	9.1 ± 0.9	2660 ± 297	8.6 ± 1.0	1.0
14	8.1 ± 0.5	10.4 ± 0.6	3689 ± 253	9.6 ± 0.7	1.1
15	8.1 ± 0.4	10.4 ± 0.4	4037 ± 214	9.9 ± 0.5	1.1
16	8.5 ± 0.3	11.0 ± 0.3	5592 ± 220	11.0 ± 0.4	1.0
17	9.7 ± 0.2	12.5 ± 0.3	7189 ± 231	12.0 ± 0.4	1.0
18	10.3 ± 0.2	13.3 ± 0.2	8239 ± 237	12.5 ± 0.4	1.1
19	10.6 ± 0.2	13.7 ± 0.2	8026 ± 222	12.4 ± 0.3	1.1
20	11.9 ± 0.2	15.4 ± 0.2	12908 ± 309	14.6 ± 0.3	1.1
21	13.7 ± 0.4	17.7 ± 0.5	15324 ± 748	15.4 ± 0.8	1.1
22	13.6 ± 0.2	17.5 ± 0.3	16189 ± 473	15.7 ± 0.5	1.1
23	13.3 ± 0.3	17.2 ± 0.3	14864 ± 638	15.3 ± 0.7	1.1
24	13.9 ± 0.3	17.9 ± 0.3	16038 ± 653	15.6 ± 0.6	1.1
25	14.7 ± 0.5	19.0 ± 0.6	18075 ± 1201	16.3 ± 1.1	1.2
26	15.0 ± 0.5	19.3 ± 0.6	17287 ± 1181	16.0 ± 1.1	1.2
27	14.6 ± 0.3	18.6 ± 0.4	15898 ± 707	15.6 ± 0.7	1.2
28[b]	15.1 ± 0.3	19.5 ± 0.4	19143 ± 864	16.6 ± 0.7	1.2
29[b]	15.5 ± 0.3	20.0 ± 0.4	20061 ± 885	16.9 ± 0.7	1.2
30[b]	15.4 ± 0.3	20.4 ± 0.4	19836 ± 808	16.8 ± 0.7	1.2
31[b]	15.5 ± 0.3	20.1 ± 0.3	21183 ± 764	17.2 ± 0.6	1.2
32	15.5 ± 0.3	20.0 ± 0.4	22218 ± 918	17.4 ± 0.7	1.1
33	15.6 ± 0.3	20.1 ± 0.4	22839 ± 905	17.6 ± 0.7	1.1
34	16.0 ± 0.3	20.6 ± 0.4	25321 ± 997	18.2 ± 0.7	1.1
35	15.8 ± 0.4	20.4 ± 0.6	27823 ± 1778	18.8 ± 1.2	1.1
36	17.0 ± 0.6	21.9 ± 0.7	36661 ± 2978	20.6 ± 1.7	1.1
37	16.2 ± 0.5	21.0 ± 0.6	38546 ± 2755	21.0 ± 1.5	1.0
38	17.5 ± 0.5	22.6 ± 0.7	38607 ± 2903	21.0 ± 1.6	1.1
39	19.8 ± 0.9	25.5 ± 1.1	71357 ± 9478	25.7 ± 3.4	1.0
40	20.6 ± 0.7	26.6 ± 0.9	84712 ± 8865	27.2 ± 2.9	1.0
41–50[a]	–	–	–	–	–

[a] No particles could be detected.
[b] These fractions were combined and used for toxicity testing.

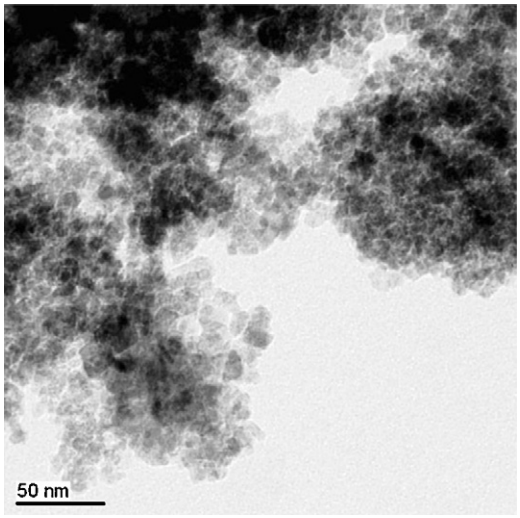

Fig. 6. TEM picture of a powder of iron oxide, Fe_2O_3, nanoparticles. The particles are spherical to a first approximation but in detail they are significantly irregularly shaped and angular. The evaluation of TEM pictures reveals radii in a range of 10–20 nm as specified by the manufacturer (reprint of the TEM picture with friendly permission from Io-Li-Tec).

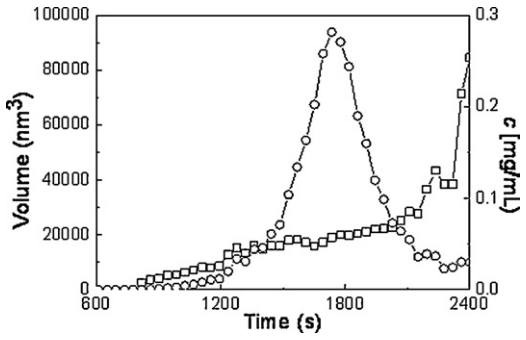

Fig. 7. Results of SAXS analysis for determination of the particle volume (squares) according to Eq. (2). Particle concentrations (circles) were determined from particle volumes, $I(0)$ values, and a concentration reference value $c = 0.244\,\mathrm{mg\,mL^{-1}}$ (Fe_2O_3) for fraction number 30 at 1800 s.

cal for engineered nanoparticles which are produced by grinding processes.

The Guinier evaluation uses only information from a small region of the scattering curve, which may produce incorrect values, for example, if the data displays systematic deviations from a straight line in a Guinier plot [28]. Therefore, additionally, calculation of the particles' volumes, V, and the corresponding radii was performed. The forward scattering $I(0)$ and Porod's invariant Q [29] allow calculation of the V from the relationship [29]

$$V = 2\pi^2 \frac{I(0)}{Q}. \quad (2)$$

The Porod invariant Q is defined as the integral

$$Q = \int_0^\infty q^2 I(q) dq, \quad (3)$$

which is experimentally available from a $q^2I - q$-plot. It is obvious from inspection of Eq. (3) that information from the entire scattering curve serves as input for the determination of the particles' volume. Note that no absolute scale of the intensity and no *a priori* information about the concentration is needed. The volumes of the particles in the different fractions range from $(2660 \pm 297)\,\mathrm{nm^3}$ to $(84712 \pm 8865)\,\mathrm{nm^3}$ (Fig. 7). The particle radii were approximately calculated from the particles' volumes under the simplification of a spherical shape by $R_V = (3 \cdot V/(4 \cdot \pi))^{1/3}$ resulting in $(8.6 \pm 1.0\,\mathrm{nm}) \leq R_V \leq (27.2 \pm 2.9\,\mathrm{nm})$. Results are summarized in Table 1 where values from both routes of analysis (R deduced from R_g and R_V deduced from V) are listed. Calculation of the R/R_V allows a direct comparison of the results from the Guinier evaluation and Porod invariant calculation. The values for R/R_V range between 1.0 and 1.2 proving that the Guinier evaluation gives identical or slightly larger radii, respectively, with a maximum deviation of 20%. This proves that the results obtained with both methods are consistent. It should be noted that the deviations towards larger values for the Guinier evaluation is conclusive because it uses only information in the low q-region.

The fractions were collected every 60 s by a fraction collector connected directly to the outlet of the SAXS flow capillary. Those fractions yielding the desired particle size and concentration were combined and used for further experiments. The mean iron content in these combined fractions was $0.244 \pm 0.006\,\mathrm{mg\,mL^{-1}}$, which is suitable for further dilution in a cell culture medium to yield nanoparticle concentrations of 5–100 $\mu\mathrm{g\,mL^{-1}}$. We determined particles concentrations by combining Eqs. (1) and (2) with the concentration of fraction 30 as reference value. The result is shown in Fig. 7.

3.3. Nanoparticles in cell assays

We applied CTB assays as a commonly used method to determine the oxidative metabolism and cell proliferation. In addition, DAPI staining was used to verify the CTB results and distinguish whether there is an increase in the metabolic activity or in the cell number. However, DAPI staining could be influenced by apoptosis, because apoptotic cells concentrate DAPI and thus could pretend a higher cell number. To avoid misinterpretation, a subsequent staining was performed in the same 96-well plates. The cells were exposed to 5, 10, 25, 50 and 100 $\mu\mathrm{g\,mL^{-1}}$ Fe_2O_3 nanoparticles of 15 nm R_g (see Table 1) and corresponding sodium polyphosphate controls in either serum free or 10% serum-containing cell culture medium for 24, 48 and 72 h. Microscopical images showed morphologically normal Caco-2 cells at all concentrations. There was no visual sign of toxicity, but a concentration-dependent orange layer of nanoparticles was observed on the Caco-2 cells (Fig. 8).

The results of the CTB assay and DAPI staining for the exposure with Fe_2O_3 nanoparticles in serum free medium are presented in Fig. 9. As shown by DAPI staining, the cell number decreases over time and with increasing particle concentration. In contrast to this the metabolic activity rises at high concentrations (50 and 100 $\mu\mathrm{g\,mL^{-1}}$) after 48 h and for lower concentrations (10 and 25 $\mu\mathrm{g\,mL^{-1}}$) after 72 h followed by a gradual decrease. Adding fetal calf serum to the incubation medium attenuated the observed effects on the cells (see Fig. 9) and elevated the variability of the measurements. Thus, there must be an influence of the serum on the nanoparticles or on the cell nanoparticle interaction.

Several studies have shown an influence of FCS on the nanoparticles and hence on the interaction of the particles with the cells, and therefore on the toxicological results [30,16,31]. These studies detected a nanoparticle stabilizing effect of fetal calf serum in cell culture media compared to media without serum. In a more sophisticated approach Horie et al. was able to detect decreasing concentrations of soluble proteins and divalent calcium ions in FCS supplemented DMEM depending on the type, the size and the concentration of the suspended metal oxide nanoparticles [32]. In their study Fe_2O_3 nanoparticles with a diameter between 20 and 40 nm adsorbed proteins and divalent calcium ions from the DMEM-FCS medium as well as other metal oxide nanoparticles. Furthermore, they were able to demonstrate an inhibitory effect of nanoparticle-

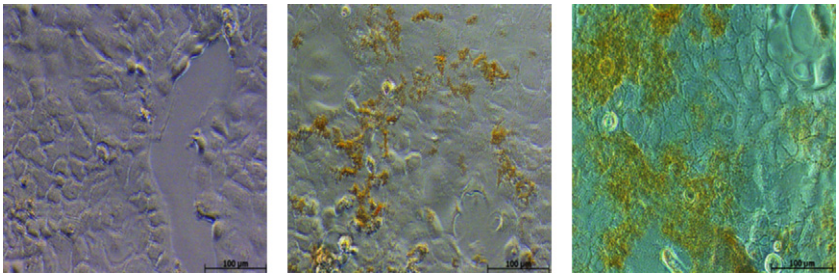

Fig. 8. Microscopical images of Caco-2 cells. 48 h treatment with serum-free medium but without nanoparticles (left) with 10 $\mu\mathrm{g\,mL^{-1}}$ (middle) and 50 $\mu\mathrm{g\,mL^{-1}}$ iron oxide nanoparticles containing serum-free medium (right) at 200-fold magnification.

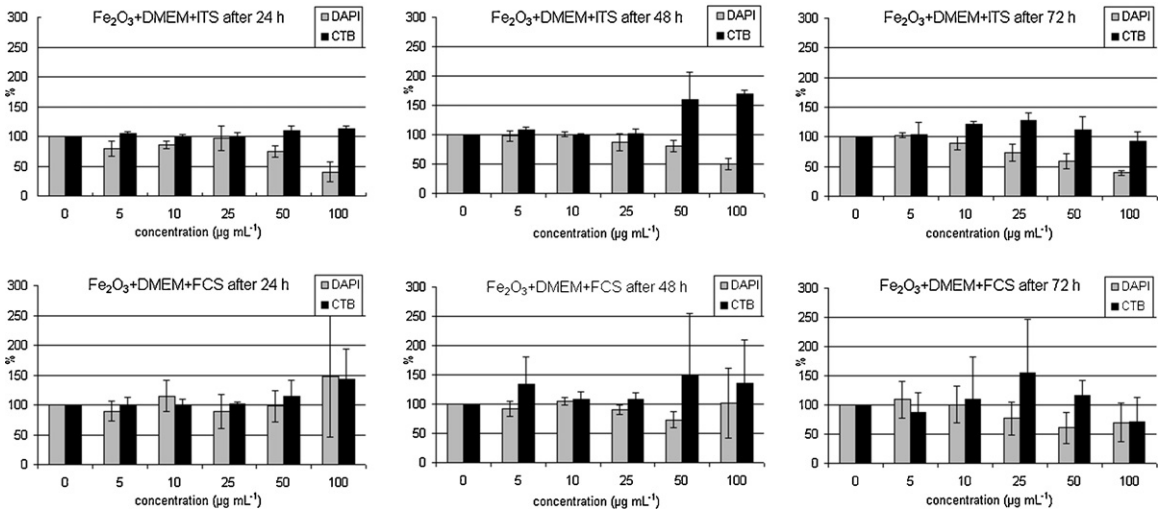

Fig. 9. Cell Titer Blue assay (CTB) and DAPI staining of Caco-2 cells with 5, 10, 25, 50 and 100 µg mL^{-1} Fe_2O_3 nanoparticles suspension for (a) 24 h, (b) 48 h and (c) 72 h incubation in serum-free (top) and serum-containing (bottom) DMEM, the results were related to corresponding sodium polyphosphate controls, and the medium control was set 100%. Differences were calculated by *f*-test and *t*-test using Microsoft Excel®.

treated media on human lung and skin cells after removal of the nanoparticles by centrifugation. This effect could be partially but not fully compensated by pretreating the suspended nanoparticles with FCS.

In our study, the inhibition of cell proliferation by Fe_2O_3 nanoparticles was more pronounced in serum-free medium than in medium containing FCS. Whether or not the effect was caused by depletion of insulin and transferrin from the medium, which could be diminished by addition of more proteins, was not determined. However, the obvious increase in the metabolic activity while growth decreased may indicate specific effects of the cell treatment with Fe_2O_3 nanoparticles in addition to protein adsorption from the medium.

Usually, hardly soluble iron oxides are presumed to have a low bioavailability and therefore a low toxicity. For this reason iron oxide pigments are permitted, e.g., as food colorants. However, reducing the size of low-solubility (Fe)-containing compounds to the nanoscale has the potential to enhance their intestinal absorption as shown by Rohner et al. for ferric pyrophosphate particles in rodent feeding studies. Increased bioavailability of a substance may increase its toxicity as well [33].

In the present study we observed inhibition of cell proliferation and finally decreased metabolic activity with and without the addition of FCS; this implies weak cytotoxic effects on a short time scale of the Fe_2O_3 nanoparticles on intestinal cells. The direct comparison of micro- and nanosized Fe_2O_3 particles by Karlsson et al. showed low toxicity for both particle types on human lung epithelial cells, but a slightly increased proportion of dead cells indicated by Trypanblue staining and increased oxidative damage indicated by the Comet Assay for the Fe_2O_3 nanoparticles [34]. These results demonstrate that the toxicity of nanoscaled materials have to be assessed separately from known substance characteristics. Additionally, the cytotoxicity of Fe_2O_3 nanoparticles on human cells depends of the cell type used in the experiments. The human mesothelioma cell line MSTO-211H is highly sensitive to Fe_2O_3 nanoparticles [35], whereas human lung epithel cells and intestinal Caco-2 cells are less sensitive.

4. Conclusion

Accurate and reliable size measurement of a given particle ensemble becomes especially important when dealing with the evaluation of safety risk assessment of certain nanoparticles. In this paper we showed that A4F-SAXS online coupling provides narrowly size-distributed fractions from a given nanoparticle sample with SAXS providing detailed information of the particles size and size distribution. With this procedure, the problem of polydispersity, which seriously affects several analytic techniques, can be overcome. Differences in reactivity and toxicity within the nanodomain of 1–100 nm can be examined. Although A4F is intended as analytical method, probing naturally low concentrated samples, it is possible to yield particle fractions after separation, which are well size-separated and ready to use in further experiments to test their effects on cells. We used Caco-2 as a well-established cell model suited for testing the impact of nanoparticles on intestinal cells. We applied CTB assays and DAPI staining as representative techniques to monitor cellular effects. For this system decrease of metabolism and cell number in dependence of concentration, time of exposure and medium composition were observed. In a further study more detailed toxicity testing especially with respect to nanoparticle characteristics in different media is projected.

We recommend the reported approach for testing the effects of nanoparticle samples in terms of their impact on cell systems with regards to size and size distribution.

Acknowledgements

We gratefully acknowledge the support from BfR and BAM.

References

[1] BUND, 2008. http://www.bund.net/fileadmin/bundnet/publikationen/nanotechnologie/20080311_nanotechnologie_lebensmittel_studie.pdf.
[2] A. Henglein, J. Phys. Chem. 97 (1993) 5457.
[3] M.F. Hochella, Earth Planet. Sci. Lett. 203 (2002) 593.
[4] P.V. Kamat, J.Phys. Chem. B 106 (2002) 7729.
[5] E.A. Corley, D.A. Scheufele, Q. Hu, J. Nanopart. Res. 11 (2009) 1573.
[6] J.M. Balbus, A.D. Maynard, V.L. Colvin, V. Castranova, G.P. Daston, R.A. Denison, K.L. Dreher, P.L. Goering, A.M. Goldberg, K.M. Kulinowski, N.A. Monteiro-Riviere, G. Oberdorster, G.S. Omenn, K.E. Pinkerton, K.S. Ramos, K.M. Rest, J.B. Sass, E.K. Silbergeld, B.A. Wong, Environ. Health Perspect. 115 (2007) 1654.
[7] A.D. Maynard, Ann. Occup. Hyg. 51 (2007) 1.
[8] A.D. Maynard, R.J. Aitken, T. Butz, V. Colvin, K. Donaldson, G. Oberdorster, M.A. Philbert, J. Ryan, A. Seaton, V. Stone, S.S. Tinkle, L. Tran, N.J. Walker, D.B. Warheit, Nature 444 (2006) 267.
[9] J.S. Tsuji, A.D. Maynard, P.C. Howard, J.T. James, C.W. Lam, D.B. Warheit, A.B. Santamaria, Toxicol. Sci. 89 (2006) 42.
[10] BfR, Stellungnahme Nr. 024/2010 des BfR vom 28.12.2009, 2010, p. 11. http://www.bfr.bund.de/cm/216/bfr_raet_von_nanosilber_in_lebensmitteln_und_produkten_des_taeglichen_bedarfs_ab.pdf.

[11] P. Buffat, J.P. Borel, Phys. Rev. A 13 (1976) 2287.
[12] K.Y. Win, S.S. Feng, Biomaterials 26 (2005) 2713.
[13] L.K. Limbach, Y.C. Li, R.N. Grass, T.J. Brunner, M.A. Hintermann, M. Muller, D. Gunther, W.J. Stark, Environ.Sci. Technol. 39 (2005) 9370.
[14] W.H. De Jong, W.I. Hagens, P. Krystek, M.C. Burger, A.J.A.M. Sips, R.E. Geertsma, Biomaterials 29 (2008) 1912.
[15] T. Schneider, Nordic Council of Ministers, 2007. ISBN 978-992-893-1563-1560. http://www.norden.org/en/publications/publications/2007-581/at_download/publicationfile.
[16] Z.P. Chen, Y. Zhang, K. Xu, R.Z. Xu, J.W. Liu, N. Gu, J. Nanosci. Nanotechnol. 8 (2008) 6260.
[17] A. Thuenemann, S. Rolf, P. Knappe, St. Weidner, Anal.Chem. 81 (2009) 5.
[18] A.F. Thunemann, J. Kegel, J. Polte, F. Emmerling, Anal.Chem. 80 (2008) 5905.
[19] J.C. Giddings, Science 193 (1976) 2.
[20] J.C. Giddings, F.J. Yang, M.N. Myers, Anal.Chem. 48 (1976) 1126.
[21] K.G. Wahlund, J.C. Giddings, Anal.Chem. 59 (1987) 1332.
[22] H. Prestel, R. Niessner, U. Panne, Anal.Chem. 78 (2006) 6664.
[23] P. Knappe, R. Bienert, S. Weidner, A.F. Thunemann, Polymer 51 (2010) 1723.
[24] A.F. Thunemann, P. Knappe, R. Bienert, S. Weidner, Anal.Meth. 1 (2009) 177.
[25] N.N. Rao, M.R. Gomez-Garcia, A. Kornberg, Ann.Rev.Biochem. 78 (2009) 605.
[26] A.B. Lampen, A. Bestmann, T. Winkler, M. Witte, L.J.T. Borlak, Xenobiotica 28 (1998) 429.
[27] S. Klenow, B.L. Pool-Zobel, M. Glei, Toxicol. In Vitro 23 (2009) 400.
[28] N. Stribeck, X-ray Scattering of Soft Matter, 1st ed., Springer, Hamburg, 2007, p. 95f.
[29] O. Glatter, O. Kratky, Small Angle X-ray Scattering, Academic Press, London, 1982, p. 153f.
[30] M. Vippola, G.C.M. Falck, H.K. Lindberg, S. Suhonen, E. Vanhala, H. Norppa, K. Savolainen, A. Tossavainen, T. Tuomi, Human Exp. Toxicol. 28 (2009) 377.
[31] A. Petri-Fink, B. Steitz, A. Finka, J. Salaklang, H. Hofmann, Eur. J. Pharm. Biopharm. 68 (2008) 129.
[32] M. Horie, K. Nishio, K. Fujita, S. Endoh, A. Miyauchi, Y. Saito, H. Iwahashi, K. Yamamoto, H. Murayama, H. Nakano, N. Nanashima, E. Niki, Y. Yoshida, Chem.Res. Toxicol. 22 (2009) 543.
[33] F. Rohner, F.O. Ernst, M. Arnold, M. Hibe, R. Biebinger, F. Ehrensperger, S.E. Pratsinis, W. Langhans, R.F. Hurrell, M.B. Zimmermann, J.Nutr. 137 (2007) 614.
[34] H.L. Karlsson, J. Gustafsson, P. Cronholm, L. Moller, Toxicol.Lett. 188 (2009) 112.
[35] T.J. Brunner, P. Wick, P. Manser, P. Spohn, R.N. Grass, L.K. Limbach, A. Bruinink, W.J. Stark, Environ.Sci. Technol. 40 (2006) 4374.